

Electron Correlation and Spin Dynamics in Iron Pnictides and Chalcogenides

Rong Yu¹, Qimiao Si¹, Pallab Goswami², Elihu Abrahams³

¹ Department of Physics and Astronomy, Rice University, Houston, Texas 77005, USA

² National High Magnetic Field Laboratory and Department of Physics, Florida State University, Tallahassee, Florida 32306, USA

³ Department of Physics and Astronomy, University of California Los Angeles, Los Angeles, CA 90095, USA

E-mail: qmsi@rice.edu

Abstract. Superconductivity in the iron pnictides and chalcogenides is closely connected to a bad-metal normal state and a nearby antiferromagnetic order. Therefore, considerable attention has been focused on the role of electron correlations and spin dynamics. In this article, we summarize some key experiments that quite directly imply strong electron correlations in these materials, and discuss aspects of the recent theoretical studies on these issues. In particular, we outline a w -expansion, which treats the correlation effects using the Mott transition as the reference point. For the parent systems, it gives rise to an effective J_1 - J_2 model that is coupled to the itinerant electrons in the vicinity of the Fermi energy; this model yields an isoelectronically-tuned quantum critical point, and allows a study of the distribution of the spin spectral weight in the energy and momentum space in the paramagnetic phase. Within the same framework, we demonstrate the Mott insulating phase in the iron oxychalcogenides as well as the alkaline iron selenides; for the latter system, we also consider the role of an orbital-selective Mott phase. Finally, we discuss the singlet superconducting pairing driven by the short-range J_1 - J_2 interactions. Our considerations highlight the iron pnictides and chalcogenides as exemplifying strongly-correlated electron systems at the boundary of electronic localization and itinerancy.

1. Introduction

Superconductivity in iron pnictides and chalcogenides [1] occurs by chemical doping of their antiferromagnetic parents, compounds in which the Fe valence is +2. The relationship between superconductivity and parent antiferromagnetism has been discussed from the beginning of the field [2]. The materials have a layered structure, with each layer containing a square lattice of Fe ions. Their electronic properties are primarily associated with the Fe 3d orbitals. The appropriate microscopic Hamiltonian contains a kinetic-energy part involving both intra- and inter-orbital hopping, as well as an interaction component featuring Coulomb repulsions and Hund's coupling.

The study of spin dynamics has played a central role in the developing understanding of the microscopic physics and the phases of these compounds. Based on the fact that the parent compounds are “bad” metals, a strong-coupling approach was advanced early on [3]. This approach expands around the Mott transition in terms of a parameter w , which measures the coherent part of electronic excitation spectrum as is depicted in Fig. 1; this parameter is small when the ratio of effective electron-electron interaction to bandwidth is large.

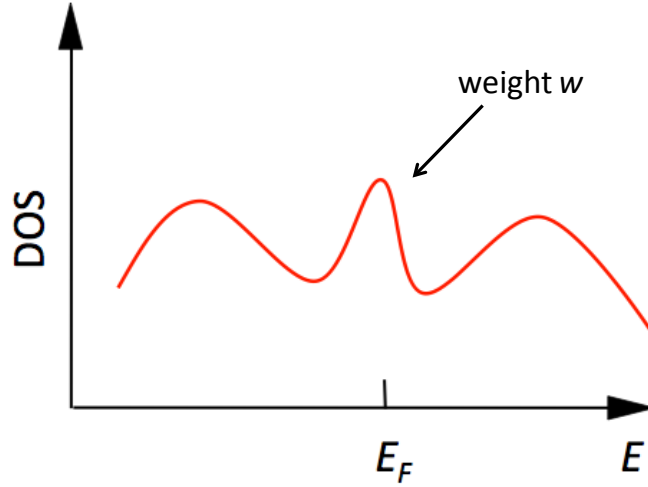


Figure 1. Single-electron spectral function as the sum of coherent and incoherent parts. The single-electron density of states (DOS) is plotted against energy (E); E_F is the Fermi energy. Each peak may contain additional structure due to the multi-orbital nature of the iron pnictides.

To zeroth order in w , the entire spectrum is incoherent and represents quasi-localized local moments and a J_1 - J_2 coupling of these local moments was proposed [3, 4]; this provided the understanding of the collinear antiferromagnetic order of the parent compounds. At higher order in w , the local moments become coupled to the itinerant carriers [3, 5, 6]. In the doped systems, the approach leads to a multiband t - J_1 - J_2 model that has been used to study the superconductivity. This is a strong-coupling approach, and is in sharp contrast to a weak-coupling description that invokes nesting of hole and electron Fermi surface pockets to drive both the spin fluctuations and superconductivity. Related strong-coupling approaches have been taken from a number of perspectives [7, 8, 9, 10, 11, 12, 13, 14, 15, 16, 17, 18, 19, 20, 21].

Here we provide a brief status report on this line of approach to the iron pnictides. We begin by expounding, in Sec. 2, on the experimental evidences for the importance of electronic correlations.

In Sec. 3, we summarize the w -expansion with respect to the Mott transition point. Sec. 4 is devoted to the magnetic quantum critical point (QCP) that arises by increasing w , which is associated with the reduction of U/W , the ratio of the direct Coulomb and Hund's exchange interactions to the characteristic bandwidth. In addition, we summarize the theoretical proposal for realizing the QCP by P-substitution for As in the parent iron pnictides, and the subsequent experimental realizations.

In Sec. 5, we consider the quantum fluctuations in the magnetic sector. For the parent iron pnictides, we show that our J_1 - J_2 based results compare well with the inelastic neutron scattering results in the parent iron pnictides. For the parent alkaline iron selenides, the predictions based on an extended J_1 - J_2 model have been confirmed by experiments.

In Sec. 6, we consider the effects of tuning the parent systems in the opposite direction, by enhancing U/W . This occurs in $\text{La}_2\text{O}_2\text{Fe}_2\text{O}(\text{Se,S})_2$, in which the expansion of the Fe square lattice leads to a Mott insulator.

In Sec. 7, we address the correlation effects in the alkaline iron selenides. The enhanced electron correlations by the ordered iron vacancies leads to Mott insulating behavior in the parent compounds. We consider how the vacancy-ordered Mott insulating parent compounds are connected to the vacancy-disordered metallic phase via a novel orbital-selective Mott phase.

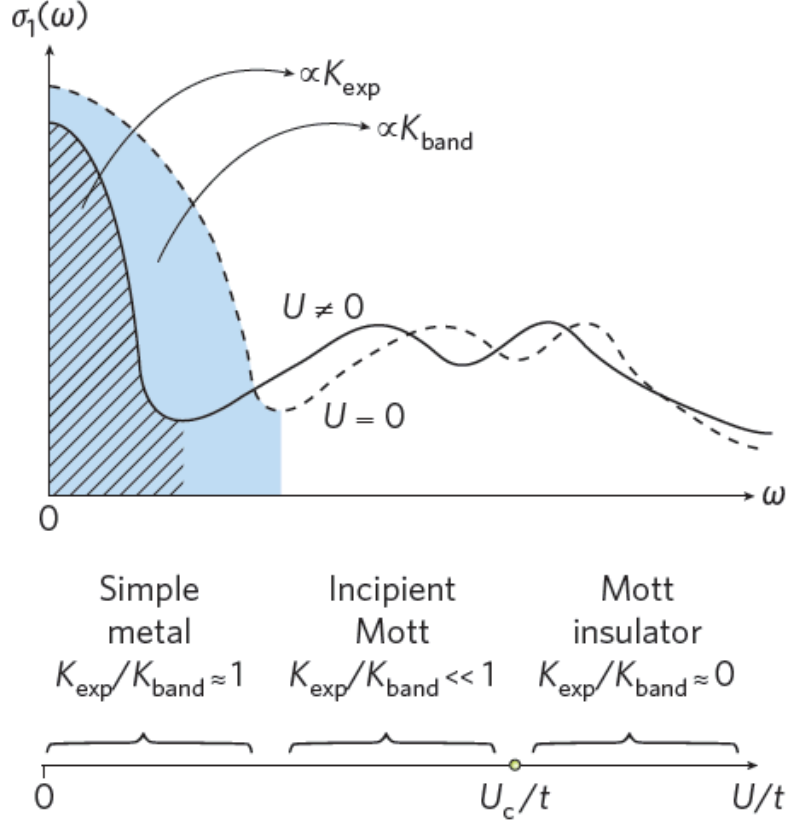


Figure 2. Electronic correlations in the undoped iron pnictides. The optical conductivity as a function of frequency. The area K under the $\omega = 0$ Drude peak is proportional to the kinetic energy of the coherent electrons near the Fermi energy. K_{exp} is measured and K_{band} , is the expected value from (non-interacting) band theory. The degree to which $K_{\text{exp}}/K_{\text{band}}$ is smaller than one is a measure of the ratio of the electron-electron repulsion to bandwidth, U/t , or a measure of the coherent quasiparticle weight w . The interaction transfers spectral weight from low energies to high energies, up to order U . U_c is the threshold interaction for a Mott localization transition. That $K_{\text{exp}}/K_{\text{band}}$ is substantially smaller than one means that U/t is smaller than but close to U_c/t , where the electrons are on the verge of losing their itinerancy.

Finally, we discuss the effect of the reduced/suppressed vacancy order on the spin spectral weight at temperatures above the Néel/structural transitions in the insulating alkaline iron selenides.

In Sec. 8, we discuss the superconducting pairing for iron pnictides and alkaline iron selenides based on the strong-coupling model. Sec. 9 includes some summary remarks.

2. Experimental manifestations of strong-coupling physics

The strong-coupling approach has its roots in a number of experimental observations. One is the fact that the room temperature resistivity is so high ($\sim 0.4 \text{ m}\Omega\text{-cm}$) that the mean free path is only of order the Fermi wavelength, as is typical for bad metals near a Mott transition. Because this is the case even in compounds that are quite pure as inferred from their small residual resistivity, it signifies the existence of strong inelastic scatterings that are attributable to the sizable electron-electron interactions [3, 22]. This arises if the metallic parent iron pnictides are

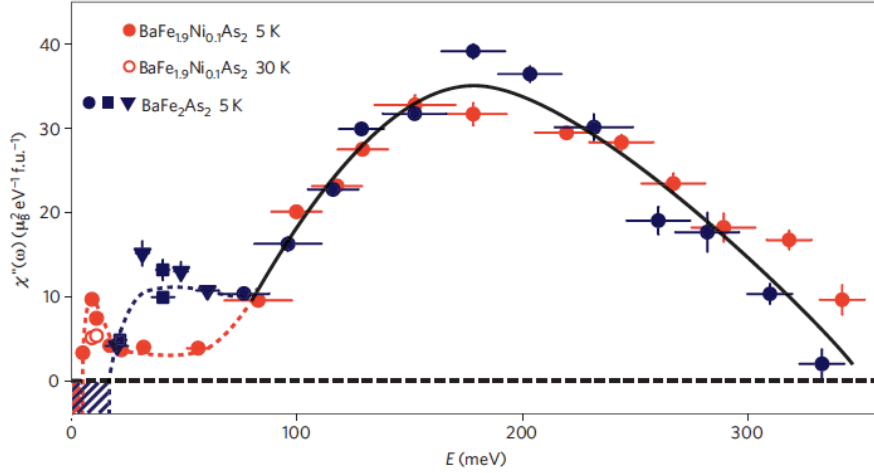


Figure 3. Spin spectral weight for several iron arsenides. Adapted with permission from Ref. [28].

close to a Mott transition, when only a small portion of the single-electron excitation spectrum lies in the coherent low-energy part, of weight w (Fig. 1).

This bad-metal interpretation has been confirmed by optical conductivity measurements [23, 24, 25, 26, 27]. As illustrated in Fig. 2, the experimentally measured spectral weight for the Drude peak normalized by the non-interacting value extracted from band-structure calculations, K_{exp}/K_{band} , provides a measure of the correlation strength: it would be close to 1 for weakly interacting systems, and close to 0 for Mott insulators. The experimentally determined value [23, 24] is close to about 1/3, falling into the regime of bad metals in proximity to Mott localization. This implies that a large portion of the single-electron spectral weight lies in the incoherent part, which would be associated with the large Coulomb (direct plus Hund's) interaction energy scale. At the same time, this reduction of Drude weight is accompanied by the transfer of optical spectral weight between low and high frequencies.

The spin dynamics, as revealed in inelastic neutron scattering experiments [28, 29, 30], also gives strong support to the picture of interacting local moments, whose sizeable spectral weight arises from the *incoherent* part (weight $\sim 1 - w$) of the electronic excitation spectrum. This is illustrated in Fig. 3, adapted from Liu et al [28], where the spin spectral distribution is shown over a range of energies which includes spin waves throughout the Brillouin zone. The integrated spectral weight is very large ($\int d\omega \chi'' \sim 3\mu_B^2$ per Fe), consistent with local moments of spin ~ 1 . Such a large spectral weight readily arises from the incoherent part of the single-electron spectral weight, as DMFT calculations have shown [28, 31, 32], but is very difficult to obtain from the single-electron excitations in the vicinity of the small Fermi pockets in the weak-coupling approaches. Indeed, an RPA calculation fails to represent the data [28].

The observation of the Mott insulating behavior in the iron oxychalcogenides [33] and vacancy-ordered alkaline iron selenides [34, 35] has provided further evidence for the strong electron correlations. These materials should be metallic according to the LDA bandstructure calculations in the paramagnetic state (even in the presence of the ordered vacancies in the alkaline iron pnictides), but are observed to be insulating with a very large ordered moment. As discussed in Secs. 6 and 7, the Mott insulating nature of these materials - as opposed to the metallic behavior of the parent iron pnictides - can be understood in terms of a reduced bandwidth but a comparable strength of the Coulomb interaction (along with the Hund's coupling). Since the reduction of the LDA bandwidth is rather modest, the observed Mott

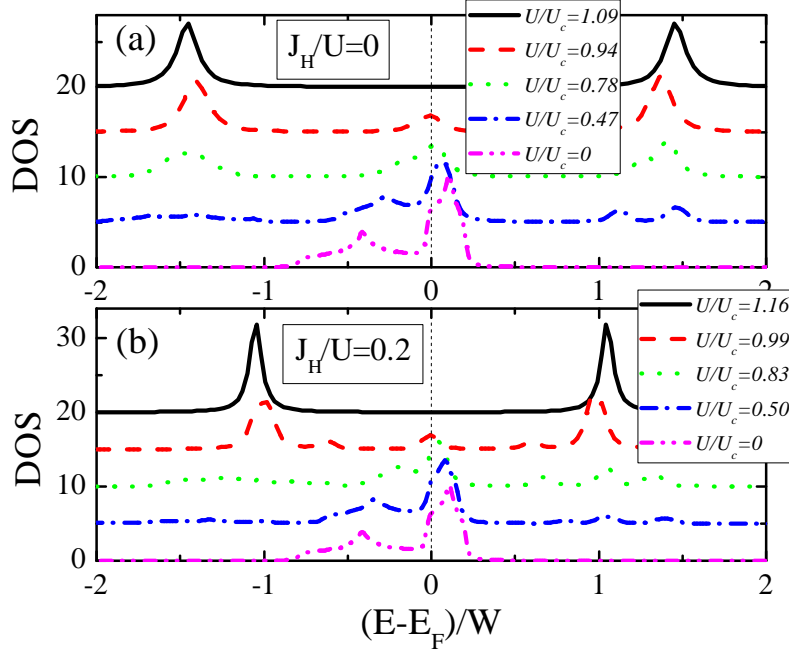


Figure 4. Density of states (DOS) of a two-orbital model derived in a slave-spin study. Results for both the zero Hund’s coupling (a) and a non-zero Hund’s coupling (b) show incoherent electronic excitations across the Mott transition, $U = U_c$. In both (a) and (b), the curves for $U/U_c > 0$ have been shifted upward for clarity. Adapted from Ref. [36].

insulating behavior provides evidence for the strong electron correlations in the iron pnictides as well. More generally, the evolution in the degree of itinerancy across the various materials families in the iron-based materials can be understood in a picture in which the strength of the local interactions (U) is fixed but the kinetic energy ($\propto W$) is variable, as can be seen through calculations of multi-orbital models [36, 37] and *ab initio* LDA+DMFT studies [7].

3. The w -expansion of a multi-orbital Hubbard model with respect to the Mott transition

For bad metals near a Mott transition, the incoherent electronic excitations play a dominant role in the spin dynamics. This effect is difficult to describe in a direct expansion of U/W , with respect to the non-interacting reference point. It can instead be more readily captured by an expansion with respect to the Mott transition point, with $(U_c - U)/W$ being the small parameter. In practice, this is equivalent to expanding in terms of w , the percentage of the single-electron spectral weight in the coherent part [3, 5, 38].

When $w = 0$, at the Mott transition, we can integrate out all the gapped single-electron excitations. The vanishing w implies the absence of the coherent spectral weight, as is already inferred in Fig. 1 and is further illustrated in Fig. 4, which shows the spectral function across the Mott transition U_c in a multi-orbital model with or without the Hund’s coupling J_H as determined using a slave-spin technique [36, 37]. This leads to localized magnetic moments, with the exchange interactions on the Fe-square lattice containing both the nearest-neighbor component J_1 and the next-nearest-neighbor one J_2 [3, 5]. General considerations suggest that $J_2 \gtrsim J_1/2$. In this parameter regime, the ground state of the $J_1 - J_2$ Heisenberg model on the square lattice is expected to have the collinear $(\pi, 0)$ antiferromagnetic order [39], as is observed

experimentally in the iron pnictides. Furthermore, the antiferromagnetic order in this model is accompanied by an Ising order, whose linear coupling to structural degrees of freedom induces a structural distortion which is also seen experimentally in the pnictides.

Because the charge gap is relatively small, we may also expect significant higher-spin couplings. Of particular interest is the four-spin biquadratic interaction K , whose effect we will discuss in Sec. 5.

At higher order in w , there are itinerant coherent carriers which are coupled to the local moments. This is summarized in the following equations for the couplings: At $w = 0$,

$$H_J = \sum_{\langle ij \rangle} J_1^{\alpha\beta} \mathbf{s}_{i,\alpha} \cdot \mathbf{s}_{j,\beta} + \sum_{\langle\langle ij \rangle\rangle} J_2^{\alpha\beta} \mathbf{s}_{i,\alpha} \cdot \mathbf{s}_{j,\beta} + \sum_{i,\alpha \neq \beta} J_H^{\alpha\beta} \mathbf{s}_{i,\alpha} \cdot \mathbf{s}_{i,\beta}, \quad (1)$$

where $\langle ij \rangle$ and $\langle\langle ij \rangle\rangle$ label nearest-neighbor (n.n.) and next-nearest-neighbor (n.n.n.) Fe sites on its square lattice. The greek indices label the orbitals and J_H is the on-site Hund's coupling. Because of the multiple orbitals, both J_1 and J_2 are matrices. At linear order in w , the kinetic energy H_c of the itinerant carriers and their coupling H_m to the quasi local moments appear when integrating out the high energy degrees of freedom:

$$H_c = w \sum_{\mathbf{k}, \alpha, \sigma} E_{\mathbf{k}\alpha\sigma} c_{\mathbf{k}\alpha\sigma}^\dagger c_{\mathbf{k}\alpha\sigma} \quad (2)$$

$$H_m = w \sum_{\mathbf{k}\mathbf{q}\alpha\beta\gamma} G_{\mathbf{k},\mathbf{q}\alpha\beta\gamma} c_{\mathbf{k}+\mathbf{q}\alpha\sigma}^\dagger \frac{\boldsymbol{\tau}_{\sigma\sigma'}}{2} c_{\mathbf{k}\beta\sigma'} \cdot \mathbf{s}_{\mathbf{q}\gamma}, \quad (3)$$

where $\boldsymbol{\tau}$ are the Pauli matrices. The final form for the low-energy effective Hamiltonian is

$$H_{eff} = H_J + H_c + H_m. \quad (4)$$

4. Quantum criticality in the iron pnictides

An important consequence of the strong-coupling approach is that by tuning the strong-coupling parameter w , one can access a QCP, separating a paramagnetic metallic phase from an antiferromagnetic or possibly insulating phase. Indeed, it was predicted [6] and subsequently experimentally confirmed that doping phosphorus into a magnetic Fe-As parent compound would reveal a magnetic quantum critical point, as shown in Fig. 4. The reason is that, since P is smaller than As, the lattice contracts a bit upon P doping, with a consequence that the kinetic energy (bandwidth) increases so that w increases to a critical value w_c at which the magnetism disappears. This can be understood by examining the action that describes the quantum fluctuations of the J_1 - J_2 model, which is appropriate when $w = 0$: $\mathcal{S} = \mathcal{S}_2 + \mathcal{S}_4 + \dots$, with

$$\mathcal{S} = \int d\mathbf{q} d\omega [r_0 + c_1 q_x^2 + c_2 q_y^2 + \omega^2 (|\mathbf{m}(\mathbf{q}, \omega)|^2 + |\mathbf{m}'(\mathbf{q}, \omega)|^2)]. \quad (5)$$

Here, $r_0 < 0$ and \mathbf{m} and \mathbf{m}' are vector order parameters describing the Néel vectors of two interpenetrating sublattices on the square lattice [with $\mathbf{m} \pm \mathbf{m}'$ respectively corresponding to the $(\pi, 0)$ and $(0, \pi)$ order]. The couplings to the itinerant fermions at finite order in w bring about added terms to this effective theory. To the linear order in w , there are two added terms:

$$\Delta\mathcal{S} = \int d\mathbf{q} d\omega [w A_{\mathbf{Q}} + \gamma |\omega| (|\mathbf{m}(\mathbf{q}, \omega)|^2 + |\mathbf{m}'(\mathbf{q}, \omega)|^2)] \quad (6)$$

The $w A_{\mathbf{Q}}$ term is positive, providing a mass shift that weakens the $(\pi, 0)$ order; when $r_0 + w A_{\mathbf{Q}} = 0$, the magnetic order disappears at a QCP. The $\gamma |\omega|$ term describes the Landau

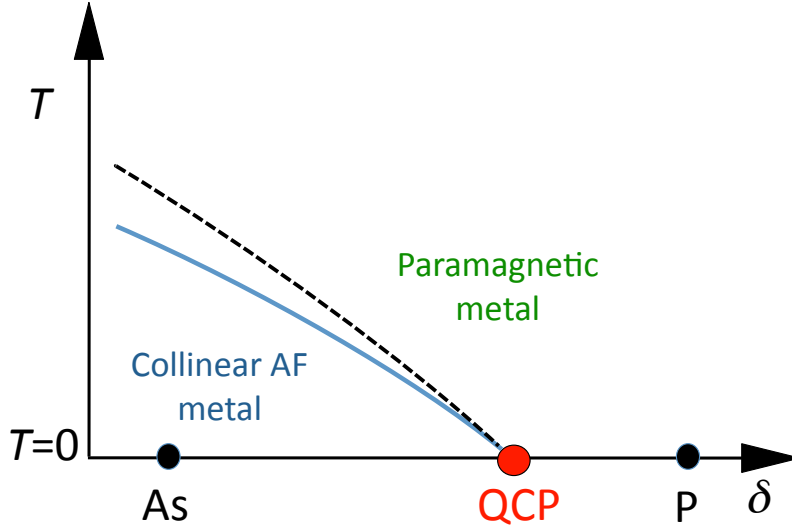


Figure 5. Pnictide phase diagram near a magnetic quantum critical point. Here δ is a non-thermal control parameter: increasing δ enhances the spectral weight w in the coherent part of the single-electron excitations. A specific example for δ is the concentration of P doping for As. The red dot denotes the quantum critical point that separates a two-sublattice collinear AF ground state from a paramagnetic one. The blue solid/black dashed lines respectively represent the magnetic/structural transitions at non-zero temperatures. Here the structural transition reflects the transition associated with the Ising order parameter, $\mathbf{m} \cdot \mathbf{m}'$. Adapted from Ref. [6].

damping; here the prefactor γ is order w^0 , but the linear-in- ω dependence has an upper cutoff frequency that is linear in w . Thus, the total $\mathcal{S} + \Delta\mathcal{S}$ gives rise to a magnetic QCP, as illustrated in Fig. 4, where at a critical value of the P-doping, $r_0 + wA_Q = 0$. An important ingredient of the analysis given in Ref. [6] is that the quartic coupling, $\tilde{u}(\mathbf{m} \cdot \mathbf{m}')^2$, is only marginally relevant with respect to the underlying fixed point associated with the $O(3)$ transition of \mathbf{m} (and \mathbf{m}'). This makes the Ising and antiferromagnetic transitions to be essentially coinciding and second order. (By contrast, for the thermally driven transition, \tilde{u} is strongly relevant with respect to the classical $O(3)$ fixed point, and the Ising and antiferromagnetic transitions become either significantly split or first order.)

This theoretical proposal for a magnetic QCP in P-doped parent iron arsenides [6] has now been extensively confirmed in experiments carried out in P-doped CeFeAsO [40, 41, 42] and BaFe₂As₂ [43, 44, 45].

5. Spin dynamics in the paramagnetic phase of parent iron pnictides

Quantum criticality represents one way to study the quantum fluctuations, through the tuning of a control parameter. Alternatively, these fluctuations can be directly probed by studying the frequency and wave-vector dependences of the spin structure factor. A particularly instructive case to consider is the parent arsenides in their paramagnetic phases, at $T > T_N$ [47, 48, 49]; the absence of order facilitates the study of the underlying interactions. With that in mind, we have studied the $J_1 - J_2 - K$ model:

$$H = J_1 \sum_{i,\delta} \mathbf{S}_i \cdot \mathbf{S}_{i,\delta} + J_2 \sum_{i,\delta'} \mathbf{S}_i \cdot \mathbf{S}_{i+\delta'} - K \sum_{i,\delta} (\mathbf{S}_i \cdot \mathbf{S}_{i,\delta})^2 \quad (7)$$

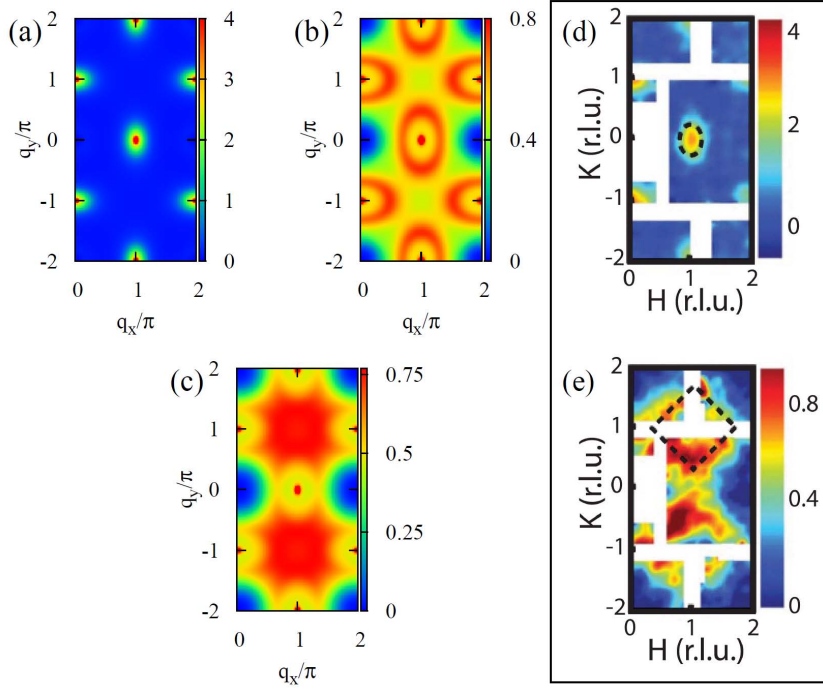


Figure 6. Evolution of the spin structure factor $S(q, \omega)$ in the paramagnetic phase of the $J_1 - J_2 - K$ model and the comparison with inelastic neutron scattering results of BaFe_2As_2 . The calculated $S(q, \omega)$ shows elliptical features near $(\pi, 0)$ at low energies (in panels (a) and (b)). They are split into features that are centered around (π, π) , as the energy is increased towards the zone-boundary spin-excitation energy (panel (c)). This trend is consistent with the inelastic neutron scattering experiments, shown in the box at the right for two energies measured in the paramagnetic phase of BaFe_2As_2 (data taken from Ref. [48]). Adapted from Ref. [50].

which is combined with the damping term specified in Eq. 6. Our approach represents one way to describe the spin dynamics by incorporating the contributions of the incoherent single-electron excitations in bad metals close to a Mott transition. An alternative approach is to study the spin dynamics in this regime using the DMFT method [31]. The results from the two approaches are complementary.

To calculate the dynamical structure factor, in Ref. [50] we have decoupled the biquadratic coupling using Hubbard-Stratonovich fields and applied a modified spin-wave method [51] to treat the resulting spin Hamiltonian. At low energies, $S(\mathbf{q}, \omega)$ as a function of \mathbf{q} displays elliptic features centered around $(\pi, 0)$ and its symmetry-equivalent points. Such elliptic features reflect the existence of two correlation lengths whose ratio is controlled by J_2/J_1 , and are not sensitive to the magnitude of the biquadratic coupling K . [Indeed, the results at low energies are similar to those for the $K = 0$ case [46].] At high energies, $S(\mathbf{q}, \omega)$ vs. \mathbf{q} is sensitive to the K coupling. Fig. 6 shows the results of the energy evolution of the momentum-distribution of the dynamical structural factor, which compares well with the experimental observations [48].

For the insulating iron alkaline iron selenides in the presence of the $\sqrt{5} \times \sqrt{5}$ vacancy order, both the block spin order and spin-wave excitations can be studied in an extended $J_1 - J_2$ model [52]. Spin-wave measurements have fully confirmed the calculated spectrum [53].

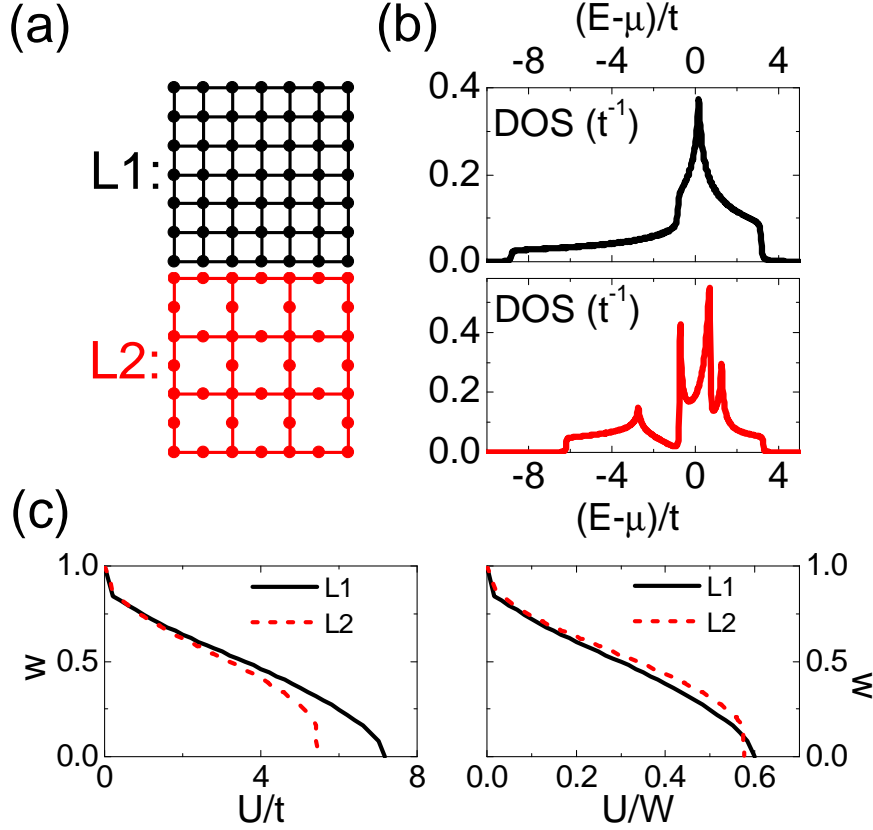


Figure 7. Kinetic energy reduction and Mott localization by ordered Fe vacancies. (a) The regular square lattice and its counterpart with 2×2 ordered vacancies (the pattern is chosen for an illustrative purpose, such that the model calculation is simplified, and similar results arise for other patterns including $\sqrt{5} \times \sqrt{5}$); (b) DOS of the two lattices; (c) Left panel: w vs. U/t . The Mott threshold U_c is reduced by the ordered vacancies. Here, t is the nearest-neighbor hopping parameter. Right panel: w plotted against U/W , showing that U_c tracks W , the bandwidth. Adapted from Ref. [54].

6. Parent Mott insulator arising from kinetic energy reduction

In Sec. 4, we discussed how to induce a QCP by increasing the kinetic energy, which increases w and weakens the magnetic order. In the same spirit, one would expect to be able to tune the system in the opposite way, by reducing the kinetic energy and thereby increasing the correlation effect. This corresponds to moving to the left on the U/t axis shown in Fig. 2.

The iron oxychalcogenides $\text{La}_2\text{O}_2\text{Fe}_2\text{O}(\text{Se},\text{S})_2$ provide a case study [33]. These are also parent compounds, *i.e.* they have a composition such that the nominal valence of Fe is 2+. They also contain an Fe square lattice, which is expanded compared to that of the iron pnictides; this leads to narrower Fe 3d-electron bands. According to LDA calculations, the paramagnetic ground state should be metallic. However, the band narrowing enhances correlation effects and promotes the Mott insulating state. Measurements of the transport and magnetic properties provide the experimental evidence that the system is indeed a Mott insulator. Because the bandwidth of $\text{La}_2\text{O}_2\text{Fe}_2\text{O}(\text{Se},\text{S})_2$ is narrower than that of the parent iron pnictides by only a moderate amount (on the order of 25%), this result provides evidence that the parent pnictides are on the verge of Mott localization. Furthermore, elastic neutron scattering measurements have determined the magnetic order [55]. and found a large ordered moment, about $2.8 \mu_B/\text{Fe}$,

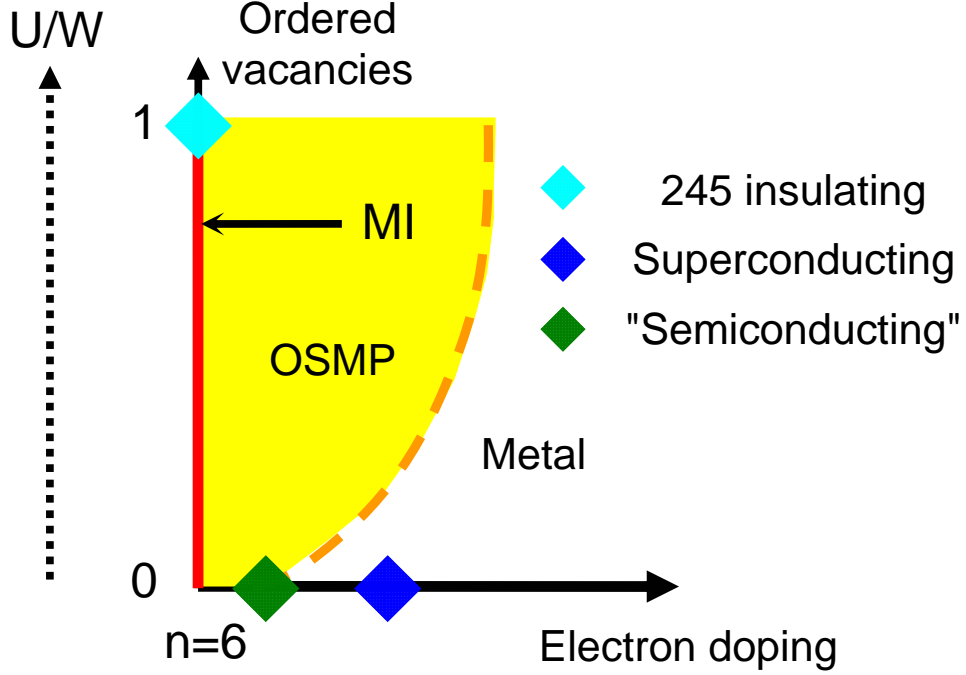


Figure 8. Overall phase diagram for $K_{1-x}Fe_{2-y}Se_2$. The vertical axis represents the degree of iron vacancy order, with 1 corresponding to fully $\sqrt{5} \times \sqrt{5}$ vacancy ordering and 0 marking complete vacancy disorder or absence of vacancies. The degree of the iron vacancy order tunes U/W . MI and OSMP stand for the Mott insulator and the orbital-selective Mott phase, respectively, and the orange dashed line describes the transition from OSMP to the delocalized metallic phase. The diamond symbols mark the approximate positions for the various phases that have been observed experimentally.

consistent with the discussion in Sec. 2.

Mott insulating behavior also exists in $R_2O_2Fe_2OSe_2$ ($R=Ce, Pr, Nd$, and Sm) which possess a similarly large ordered moment [56] and in several other iron oxychalcogenides whose ordered moments are yet to be determined: $(Sr, Ba)_2F_2Fe_2O(Se, S)_2$ (Ref. [57]), $Na_2Fe_2OSe_2$ (Ref. [58]), and $BaFe_2OSe_2$ (Refs. [59, 60]).

7. Alkaline iron selenides: Mott insulator and orbital-selective Mott insulator

Recently, superconductivity with T_c comparable to the iron pnictides was discovered in $K_{1-y}Fe_{2-x}Se_2$ ("KFS") [61] and related iron selenides with K replaced by Rb, Cs, or Tl [34, 62, 63]. Here too, the superconductivity occurs near antiferromagnetic order [34]. Angle-resolved photoemission (ARPES) experiments [64, 65, 66] have shown that the Fermi surface has only electron pockets, in contrast to the iron pnictides, which have both electron and hole pockets.

The parent selenide compounds, with Fe valence at $2+$, are insulating [34, 67]. These compounds have Fe vacancies forming ordered patterns [34, 68]. LDA band-structure calculations show that the paramagnetic ground state of such a vacancy-ordered structure is metallic [69, 70], therefore the insulating ground state must result from electron interactions. How strong are these interactions? A clue is provided by the size of the ordered moment, which is about $3.3 \mu_B/Fe$ [68, 53]. Recognizing that the maximal possible moment is $4 \mu_B/Fe$, the observed ordered moment is indeed very large. Therefore, the interaction energy must be sizable

compared to the kinetic energy.

Microscopic considerations have suggested that the Mott insulating nature of the vacancy-ordered system is very natural [54]. The ordered vacancies lead to a band-narrowing, which enhances the ratio U/W , and pushes the system to the Mott insulator side. This is shown in Fig. 7, with an illustrative model having a 2×2 vacancy ordering pattern [54].

In these iron-based compounds, there are five $3d$ orbitals which are non-degenerate; a slave-spin study [71] has identified an orbital-selective Mott phase (“OSMP”) in which the xy orbitals are localized and the remaining $3d$ orbitals are delocalized. ARPES measurements in the superconducting compound have shown that raising the temperature causes a suppression of the spectral weight of the xy orbitals near the Fermi energy, while keeping the weight of its xz and yz counterparts non-zero [72]. Combining the ARPES results and the theoretical phase diagram yields an overall phase diagram shown in Fig. 8.

The OSMP provides the link between the vacancy-ordered/Mott insulating phase and the vacancy disordered/free superconducting phase. Experimental evidence has come from transport measurements in the insulating alkaline iron selenides under pressure [73].

We close this section by discussing the expected paramagnetic spin excitations in the insulating $\text{Rb}_{0.8}\text{Fe}_{1.6}\text{Se}_2$. Because T_N is very large (on the order of 500 K), and is only slightly (a few 10’s K) below the vacancy ordering temperature T_s , the $\sqrt{5} \times \sqrt{5}$ iron vacancy order becomes fragile above T_N [68]. As we have just discussed in this section, the reduction of the iron vacancy order leads to an effective reduction of the electron correlation strength U/W from that of the fully vacancy-ordered case, destabilizing the Mott insulating state. Correspondingly, the spin spectral weight will be reduced from the very large value in the fully vacancy-ordered state. This has recently been observed: Above the Néel temperature, Wang et al. [74] reported spin excitations that are more strongly damped than those of the fully vacancy-ordered state as well as a significant reduction of the total moment. In other words, the experimental observations in the paramagnetic regime, both below and above the vacancy ordering temperature, are consistent with the Mott-insulating behavior of the fully vacancy-ordered state. The fact that the magnetic excitations at low temperatures are well described by spin waves with a very large stiffness constant reinforces the Mott-insulating behavior of the fully vacancy-ordered state.

8. Superconductivity in iron pnictides and alkaline iron selenides

In the carrier doped case, the w -expansion discussed earlier leads to a 5-band $t - J_1 - J_2$ model [5, 3]. Spin-singlet superconducting pairing from this model was studied in Ref. [75] in the case of the iron pnictides. Magnetic frustration by itself leads to a large degeneracy in the pairing states. The kinetic energy breaks this into a quasi-degeneracy among a reduced set of pairing states, as shown in Fig. 9. For small electron and hole Fermi pockets, an A_{1g} $s_{x^2-y^2}$ state dominates over the phase diagram but a B_{1g} $d_{x^2-y^2}$ state is close by in energy; an $A_{1g} + iB_{1g}$ state, which breaks time-reversal symmetry, occurs at low temperatures in part of the phase diagram. Compared to the two-band case, there is an enhanced amplitude for the A_{1g} $s_{x^2+y^2}$ channel, which causes anisotropy of the gap on the electron pockets or even an accidental gap near M .

An important advantage of this strong-coupling approach is that it gives rise to pairing amplitudes for the alkaline iron selenides that are comparable to those for the iron pnictides, in spite of the very different Fermi surfaces. This is consistent with the fact that the superconducting transition temperatures are very similar.

9. Summary and outlook

We have summarized the phenomenological basis for strong electron correlations in the iron pnictides and chalcogenides. Chief among these are the bad-metal behavior seen in the electrical transport and charge dynamics properties in both classes of materials; the large spectral weight

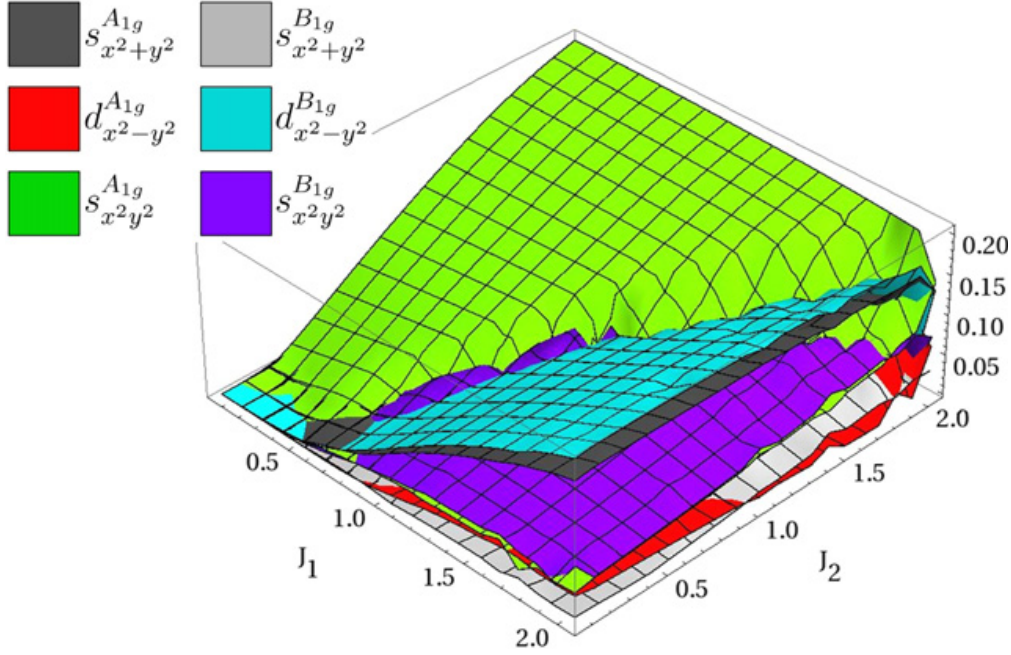


Figure 9. The pairing amplitudes (for d_{xz} , d_{yz} orbitals) in the five orbital model for electron doping $\delta = 0.14$. Adapted from Ref. [75].

observed through spin dynamics measurements, also seen in both cases; and the observation of Mott insulating states in the iron oxychalcogenides and alkaline iron selenides.

We have also outlined a w -expansion, which uses the Mott transition as a reference point. This expansion treats the bad-metal behavior through a proximity to the Mott transition, which separates the single-electron excitations into coherent and incoherent ones whose weights are w and $1 - w$ respectively. In this way, it naturally incorporates the large spin spectral weight in the bad-metal (*i.e.*, small w) regime.

For the parent arsenides, this expansion gives rise to an effective spin Hamiltonian in the form of a J_1 - J_2 model that is coupled to the itinerant electrons in the vicinity of the Fermi energy. Varying w amounts to tuning the relative degree of itinerancy vs. localization and provides a means to vary the strength of magnetic ordering. We have discussed an early theoretical proposal for a quantum critical point resulting from w -tuning and for its realization through a P-for-As isoelectronic substitution in the parent iron arsenides. This prediction has since been experimentally confirmed by a number of groups using transport, neutron, NMR and quantum oscillation measurements. Using the same approach, theoretical studies have been carried out for the spin dynamics in the paramagnetic phase of the parent arsenides. In the presence of a biquadratic interactions, the theoretical results compare well with the inelastic neutron scattering results above T_N , both at low energies near the magnetic-zone centers and at high energies close to the magnetic-zone boundaries.

We have also demonstrated how a Mott insulating phase may arise from a kinetic-energy reduction, and its experimental evidence in both the iron oxychalcogenide compounds and the vacancy-ordered alkaline iron selenides. In the latter families, we show how an orbital-selective Mott phase appears in the phase diagram.

Finally, we have discussed the singlet superconducting pairing driven by the short-range J_1 - J_2 interactions. For the carrier-doped cases, the w -expansion gives rise to a five-orbital matrix

t - J_1 - J_2 model. In this model, the dominant pairing channels are the nearly degenerate A_{1g} $s_{x^2-y^2}$ and B_{1g} $d_{x^2-y^2}$ states, with A_{1g} $s_{x^2+y^2}$ channel also playing a significant role in the iron pnictides.

More generally, we have highlighted the phenomenological and theoretical evidences that the iron pnictides and chalcogenides are bad metals at the boundary between electronic localization and itinerancy. As such, these materials not only are important in their own right, but also provide a setting to study the physics in this important parameter regime of strongly correlated electrons in general.

Acknowledgments

We are grateful to J. Dai, A. H. Nevidomskyy, P. Nikolic, Z. Wang and J.-X. Zhu for collaborations, and to them as well as many other colleagues for useful discussions. This work has been in part supported by the NSF Grant No. DMR-1006985 and the Robert A. Welch Foundation Grant No. C-1411. P. G. was supported at the National High Magnetic Field Laboratory by NSF Cooperative Agreement No. DMR-0654118, the State of Florida, and the U. S. Department of Energy. Part of this work was carried out at the Aspen Center for Physics (NSF grant 1066293).

References

- [1] Kamihara Y, Watanabe T, Hirano M, and Hosono H 2008 *J. Am. Chem. Soc.* **130** 3296
- [2] de la Cruz C et al 2008 *Nature* **453** 899
- [3] Si Q and Abrahams E 2008 *Phys. Rev. Lett.* **101** 076401
- [4] Yildirim T 2008 *Phys. Rev. Lett.* **101** 057010
- [5] Si Q, Abrahams E, Dai J, and Zhu J-X 2009 *New J. Phys.* **11** 045001
- [6] Dai J, Si Q, Zhu J-X, and Abrahams E 2009 *Proc. Natl. Acad. Sci.* **106** 4118
- [7] Yin Z P, Haule K and Kotliar G 2011 *Nat. Mater.* **10**, 932
- [8] Seo K, Bernevig B A and Hu J 2008 *Phys. Rev. Lett.* **101**, 206404
- [9] Chen, W-Q, Yang, K-Y, Zhou, Y and Zhang, F-C 2009 *Phys. Rev. Lett.* **102**, 047006
- [10] Moreo A, Daghofer M, Riera J A and Dagotto E 2009 *Phys. Rev. B* **79**, 134502
- [11] Berg E, Kivelson S A and Scalapino D J 2009 *New J. Phys.* **11**, 085007
- [12] Lv W, Krüger F and Phillips P 2010 *Phys. Rev. B* **82**, 045125
- [13] Ma F, Lu Z-Y and Xiang T 2008 *Phys. Rev. B* **78** 224517
- [14] Han M J, Yin Q, Pickett W E and Savrasov S Y 2009 *Phys. Rev. Lett.* **102** 107003
- [15] Wysocki A L, Belashchenko K D and Antropov V P 2011 *Nat. Phys.* **7** 485
- [16] Fang C, Yao H, Tsai W-F, Hu J and Kivelson S A 2008 *Phys. Rev. B* **77** 224509
- [17] Xu C, Muller M and Sachdev S 2008 *Phys. Rev. B* **78**, 020501(R)
- [18] Uhrig G S, Holt M, Oitmaa J, Sushkov O P and Singh R R P 2009 *Phys. Rev. B* **79**, 092416
- [19] Ishida H and Liebsch A 2010 *Phys. Rev. B* **81** 054513
- [20] Giannetti G, Ortix C, Marsman M, Capone M, van den Brink J and Lorenzana J 2011 *Nat. Commun.* **2** 398
- [21] Calderón M J, Le'on G, Valenzuela B and Bascones E 2012 *Phys. Rev. B* **86** 104514
- [22] Abrahams E, Si Q 2011 *J. Phys.: Condens. Matter* **23** 223201
- [23] Qazilbash M et al 2009 *Nat. Phys.* **5** 647
- [24] Hu W Z et al 2008 *Phys. Rev. Lett.* **101** 257005
- [25] Yang J et al 2009 *Phys. Rev. Lett.* **102** 187003
- [26] Boris A V et al 2009 *Phys. Rev. Lett.* **102** 027001
- [27] Degiorgi L 2011 *New J. of Phys.* **13** 023011
- [28] Liu M et al 2012 *Nat. Phys.* **8** 376
- [29] Zaliznyak I A et al 2011 *Phys. Rev. Lett.* **107** 216403
- [30] Zhao J et al 2009 *Nat. Phys.* **5** 555
- [31] Park H, Haule K, and Kotliar G 2011 *Phys. Rev. Lett.* **107** 137007
- [32] Toschi A, Arita R, Hansmann P, Sangiovanni G, and Held K 2012 *Phys. Rev. B* **86** 064411
- [33] Zhu J-X et al 2010 *Phys. Rev. Lett.* **104** 216405
- [34] Fang M et al 2011 *Euro. Phys. Lett.* **94** 27009
- [35] Wang D M, He J B, Xia T-L and Chen G F 2011 *Phys. Rev. B* **83** 132502
- [36] Yu R and Si Q 2011 *Phys. Rev. B* **84** 235115

- [37] Yu R and Si Q 2012 *Phys. Rev. B* **86** 085104
- [38] Moeller G, Si Q, Kotliar G, Rozenberg M, and Fisher D S 1995 *Phys. Rev. Lett.* **74** 2082
- [39] Chandra P, Coleman P, and Larkin A I 1990 *Phys. Rev. Lett.* **64** 88
- [40] de la Cruz C et al 2010 *Phys. Rev. Lett.* **104** 017204
- [41] Luo Y et al 2010 *Phys. Rev. B* **81** 134422
- [42] Jesche A, Krellner C, de Souza M, Lang M, and Geibel C 2009 *New J. Phys.* **11** 103050
- [43] Jiang S et al 2009 *J. Phys. Condens. Matter* **21** 382203
- [44] Kasahara S et al 2010 *Phys. Rev. B* **81** 184519
- [45] Hashimoto K et al 2012 *Science* **336** 1554
- [46] Goswami P, Yu R, Si Q and Abrahams E 2011 *Phys. Rev. B* **84** 155108
- [47] Diallo S O et al 2010 *Phys. Rev. B* **81** 214407
- [48] Harriger L W et al 2011 *Phys. Rev. B* **84** 054544
- [49] Ewings R A et al 2011 *Phys. Rev. B* **83** 214519
- [50] Yu R et al 2012 *Phys. Rev. B* **86** 085148
- [51] Takahashi M 1989 *Phys. Rev. B* **40** 2494
- [52] Yu R, Goswami P, Si Q 2011 *Phys. Rev. B* **84** 094451
- [53] Wang M et al 2011 *Nat. Commun.* **2** 580
- [54] Yu R, Zhu J-X, and Si Q 2011 *Phys. Rev. Lett.* **106** 186401
- [55] Free D G and Evans J S O 2010 *Phys. Rev. B* **81** 214433
- [56] Ni N, Jia S, Huang Q, Climent-Pascual E and Cava R J 2011 *Phys. Rev. B* **83** 224403
- [57] Kabbour H et al 2008 *J. Am. Chem. Soc.* **130** 8261
- [58] He J B, Wang D M, Shi H L, Yang H X, Li J Q and Chen G F 2011 *Phys. Rev. B* **84** 205212
- [59] Han F, Wan X, Shen B and Wen H-H 2012 *Phys. Rev. B* **86** 014411
- [60] Lei H, Ryu H, Warren J, Frenkel A I, Ivanovski V, Cekic B and Petrovic C *arXiv:1206.5788*
- [61] Guo J et al 2010 *Phys. Rev. B* **82** 180520
- [62] Krzton-Maziopa A et al 2011 *J. Phys.: Condens. Matter* **23** 052203
- [63] Mizuguchi Y et al 2011 *Appl. Phys. Lett.* **98** 042511
- [64] Zhang Y et al 2011 *Nat. Mater.* **10** 273
- [65] Qian T et al 2011 *Phys. Rev. Lett.* **106** 187001
- [66] Mou D et al 2011 *Phys. Rev. Lett.* **106** 107001
- [67] Wang D M, He J B, Xia T-L, and Chen G F, 2011 *Phys. Rev. B* **83** 132502
- [68] Bao W et al 2011 *Chin. Phys. Lett.* **28** 086104
- [69] Cao C and Dai J 2011 *Phys. Rev. Lett.* **107** 056401
- [70] Yan X-W et al 2011 *Phys. Rev. B* **83** 233205
- [71] Yu R and Si Q 2012 *arXiv:1208.5547*
- [72] Yi M et al 2012 *arXiv:1208.5192*
- [73] Gao P et al 2012 *arXiv:1209.1340*
- [74] Wang M et al 2012 *arXiv:1211.7328*.
- [75] Goswami P, Nikolic P, and Si Q 2010 *EuroPhys. Lett.* **91** 37006